



Mechanism Damage to Mode-I Fractured Sandstone from Chemical Solutions and Its Correlation with Strength Characteristics

TIELIN HAN,^{1,2}  JUNPING SHI,² YUNSHENG CHEN,² and XIAOSHAN CAO²

Abstract—The fracture toughness of rock is very important in rock cutting, blasting, and hydraulic fracturing for tunnel excavation. To evaluate factors that reduce rock fracture toughness, we emulated the environment of joint rock in the hydro-fluctuation belt of a typical bank slope in the Shanxi Tong Chuan reservoir region. We tested long-term immersion of sandstone samples in different chemical solutions to determine the resulting mechanical characteristics and damage degradation. Variations in the physical and mechanical properties of the samples were analyzed under the effects of the chemical solutions. Experimental results show that the sandstone was significantly damaged by the chemical solutions, but its peak strain increased, and different chemical solutions had distinct influences on the degree of mechanical damage. These differences varied with the acid–base properties of the solutions. Also, there were clear consistencies among the solutions in the degree of their damage to mechanical parameters, physical parameters, and ion concentrations. Therefore, we were able to obtain correlations among the physical and mechanical parameters of the sandstone samples, damage variables, and the ion concentrations of calcium and magnesium. The surfaces of the samples were seriously degraded after being subjected to the corrosive effect of various chemicals; for example, there were different amounts of holes and pitting corrosion. The sizes of the holes and the degree of surface pitting gradually increased with an increase in corrosion time.

Key words: Chemical erosion, correlation, jointed rock mass, mechanical characteristics, mode-I fracture, toughness, rock mechanics.

1. Introduction

Rocks form the main body of the lithosphere and comprise an aggregate of mineral particles, pores, and cementing materials. Microcracks, flaws, and

crevices of various orders are always scattered throughout rock. Research shows that rock failure is closely related to fractures, and deformation and failure are caused by randomly distributed internal defects that propagate, converge, and cut through the rock. Therefore, many scholars have used the fracture toughness of rocks to quantitatively evaluate the stability and safety of rock involved in engineering projects. For example, determining the ability of a rock that contains a crack to resist fracturing is very important in work that involves rock cutting, blasting, or hydraulic fracturing for tunnel excavation.

Due to the world's rapid economic development, underground resources are becoming increasingly scarce. This has led to the development of geothermal energy, oil, gas, and other energy from deep strata mining using blasting and hydraulic fracturing. For these purposes, an understanding of rock fracture toughness is increasingly important. Therefore, there has been much research in this field, with many useful results of rock fracture toughness tests having been obtained.

Brown and Reddish (1997) did an experimental study of the effects of density on the fracture toughness of rock. Zhang and Wang (2009) studied the fracture toughness of marble using five different disk-shaped specimens and obtained fracture toughness formulas for specimens of various shapes by using finite element analysis. They also compared the advantages and disadvantages of this type of testing. Saadaoui et al. (2000) and Ciccotti et al. (2000) studied the fracture toughness of rock using the double-torsion method. Chen et al. (2001) studied the effects of confining static pressure on rock fracture toughness and improved the efficiency of fracturing design and fracture prediction. Ayatollahi and Aliha

¹ Shenzhen University Guangdong Provincial Key Laboratory of Durability for Marine Civil Engineering, Shenzhen 518060, China. E-mail: s3050210133@163.com

² Institute of Geotechnical Engineering, Xian University of Technology, Xi'an 710048, Shaanxi, China.

(2007) studied the fracture toughness of brittle rock subjected to mixed mode-I and mode-II loading. Chen and Zhang (2004) did laboratory measurements and interpretation of the fracture toughness of rock formations at great depth. Wang, Feng, et al. (2011) measured dynamic fracture toughness for mode-I and mode-II using flattened Brazilian disk specimens cracked straight through then impacted by a split Hopkinson pressure bar. Cui et al. (2010) compared two chevron-notched specimens suggested by the International Society for Rock Mechanics for testing mode-I rock fracture toughness. Erarslan and Williams (2012) studied the damage mechanism of rock fatigue and its relation to fracture toughness. Zhang et al. (2008) experimentally studied the effects of rock size on fracture toughness under dynamic conditions, and Zhang (2002) experimentally studied the correlation between fracture toughness and tensile strength. As mentioned above, our research was focused mainly on the fracture toughness of different kinds of rock and the correlation between its strength parameters under static and dynamic conditions.

The hydrochemical environment is another active factor affecting the failure characteristics of rock. Water–rock interaction and chemical solution corrosion aggravate damage to rock. Most geological hazards are associated with groundwater; for example, landslides, dangerous rock, collapses, karst collapse, and land subsidence. Water–rock interaction, a key active factor, affects the safety and stability of rock-mass engineering projects. Groundwater is also often involved in the deformation and destruction of rock masses and seriously affects their mechanical characteristics. In essence, the microstructure of rock changes due to water–rock interaction, which can cause its macroscopic mechanical properties to deteriorate and leads to the failure of rock masses. As environmental pollution problems become more serious, more and more scholars have focused on this research field. Meanwhile, as studies of water–rock interaction and the intersection of multiple disciplines have increased, researchers have gradually realized that it is necessary to consider the complex stress corrosion of water–rock mixtures, instead of considering only chemical interactions between water and rock.

Water–rock reactions have advanced to the forefront of basic research topics, yielding many useful results. Heggheim et al. (2005) studied the weakening variable of the mechanical characteristics of limestone immersed in seawater. Chen et al. (2010) systematically studied the effects of hydrochemical solutions on the surface morphology of rock. Wu (2013) studied the time-varying characteristics of sandstone subjected to chemical solutions. Négrel et al. (2010) focused on the study of granite parent rock, isotopic tracers, and water chemistry, and measured the lead isotopes in the water through multicollector inductively coupled plasma mass spectrometry. Feng et al. (2001) and Li et al. (2003) did an experimental study on the effects of different chemical solutions on rock and established corresponding damage variables and constitutive relations. Vezzù et al. (2008) did a numerical simulation of the single failure of granite with and without salt pore water under axial compression. Feng et al. (2008) presented several experimental results from their investigation of the mechanism of multicroack interactions. Their study involved limestone with two or three flaws in different arrangements under coupled uniaxial compressive stress and various chemical solutions. Nara et al. (2012) studied the effect of humidity on rock fracture toughness, and Reinhardt and Mielich (2014) explored the effects of different chemical solutions on rock fracture toughness. As mentioned above, a chemical solution has a clear weakening effect on the fracture characteristics of rock. However, there are still problems with studying the fracture toughness of rock undergoing chemical corrosion and its correlation with strength parameters.

Given the research described above, and considering the actual environment of joints in rock, we adopted a test of long-term immersion to explore the mechanical parameters of mode-I fractured sandstone in a three-point bending test, a tensile test, an axial compression test, and a triaxial compression test. We also studied the effect of chemical damage on the mechanical properties of mode-I fractured sandstone and its correlation with strength characteristics. Finally, for various durations of immersion in chemical solutions, we analyzed the variations in the ion concentration, the P-wave velocity, and physical

properties of sandstone subjected to various chemical solutions. This study will serve as a reference for the development and construction of rock-mass engineering projects in reservoir regions.

2. Materials and Methods

2.1. Specimen Preparation

Calcareous sandstone was collected from a typical bank slope in the Shanxi Tongchuan reservoir region of China. The density of the specimens ranged from 2.54 to 2.56 g/cm³, and the P-wave velocity ranged from 3703 to 3791 m/s. The range of porosity was 5.36 to 5.65%. Microscopic images of the sandstone specimens are shown in Fig. 1.

Currently, there are many ways to measure rock fracture toughness. We measured the fracture toughness K_{Ic} of straight-incision cuboid sandstone with mode-I fractures strictly according to accepted guidelines (The Professional Standard Compilation Group of People's Republic of China, DL/T5368 2007) using a three-point bending method. Figure 2 shows the loading diagram, where B is the specimen width (in cm), which is equal to the specimen height W (in cm); S_d is the distance between two supporting points (in cm); P_{max} is the load leading to fracture failure (in N); and a is the depth of the straight incision (in cm). The cross sections were square with an area of 50 × 50 mm² and a height of 250 to

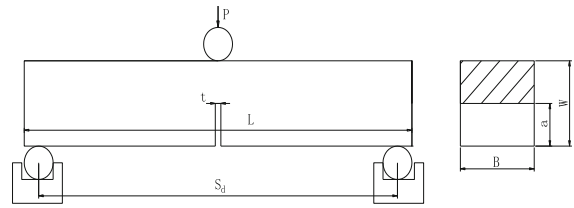


Figure 2

Loading sketch of three-point bending specimens. B denotes the specimen width (cm), which is equal to the specimen height W (cm); S_d represents the distance between two supporting points (cm); P_{max} denotes the load leading to the fracture failure (N); a is the depth of straight incision (cm)

260 mm. The depth of the straight incision was 21 to 23 mm, and its width was 1.0 mm.

P-wave velocity was measured by an acoustic wave detector (RSM-SY5) developed by the Institute of Rock and Soil Mechanics, Chinese Academy of Sciences, Wuhan, China. A total of 276 sandstone specimens were selected and divided into 21 groups. One group was used to measure fracture toughness, tensile strength, and uniaxial compression strengths of the specimens under natural conditions. The remaining 20 groups were used to experimentally study the effects of various chemical solutions.

2.2. Preparation of Chemical Solutions

Existing research shows that rock-mass engineering projects in reservoir dams, coastal areas, and inland saline lakes are often subjected to sulfate erosion, and in China, acid rain exists mainly in the

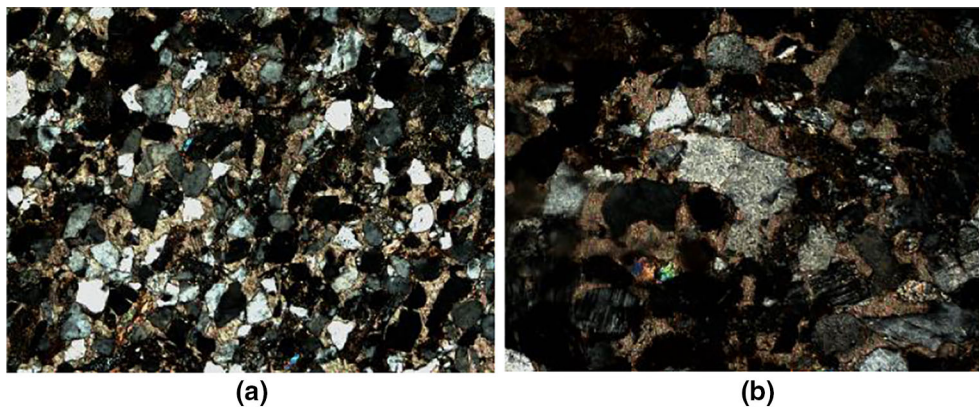


Figure 1

Microscope image of sandstone specimens. **a** Quartz and carbonate cement. **b** Carbonate pore-type cementation

form of sulfate. In rock-mass engineering projects in the Shanxi Tong Chuan reservoir region of China, the main ion composition of reservoir water is SO_4^{2-} , Cl^- , Na^+ , K^+ , HCO_3^- , and so forth, and the pH range of the reservoir water is 5.10 to 8.23. In addition, damage to the rock mass, which generates and accumulates until destruction, is a long and slow process. To observe these changes in a relatively short time, we chose lower or higher pH values of chemical solutions to carry out the research. Consequently, we chose sodium sulfate (Na_2SO_4) as a corrosion compound. The selected pHs of the sulfate solutions were 3.0 and 12.0, and we used the mechanical parameters of sandstone specimens immersed in neutral sodium sulfate (Na_2SO_4) as a reference. Each chemical solution was reconfigured monthly to maintain its initial concentration and pH. The initial acidity and basicity of the Na_2SO_4 solutions were controlled by 0.01 mol/L sodium hydroxide and 0.01 mol/L sulfuric acid solutions using a PHS-3C acidimeter (Baoshishan, China; shown in Fig. 3).

2.3. Test Methods

Before the test, the sandstone specimens were dried at 105 °C for 24 h to maintain a constant weight and then cooled for mass measurement. Next, the specimens were sealed using a vacuumization method and soaked in the following chemical solutions: 0.01 mol/L Na_2SO_4 (pH = 3.0), 0.01 mol/L



Figure 3

Sketch map of PHS-3C acidity meter and calibration liquid

Na_2SO_4 (pH = 7.0), and 0.01 mol/L Na_2SO_4 (pH = 12.0). The volume of chemical solutions used for soaking was 5.0 L. Room temperature (20 °C) was maintained throughout the experiment.

The mechanical experiments were done after measuring the P-wave velocity, and four tests were done in parallel for each month in various chemical solutions. The remaining specimens were immersed in the corresponding chemical solutions again. Meanwhile, Ca^{2+} and Mg^{2+} ion concentrations dissolved in chemical solutions were measured by using a TAS-990 atomic absorption spectrophotometer (Beijing Purkinje General Instrument Co., China), and the surfaces of the sandstone specimens were observed using an XTL-100E stereomicroscope (GX Microscopes, UK). We tested the sandstone specimens after 1, 2, 3, 4, and 5 months of immersion. Specimens not corroded by chemical solutions were used as a control group; experimental results from this group were used to represent those of specimens under 0 months and could then be compared with the experimental results of the corroded samples.

To study the relation between fracture toughness and strength, it was necessary to reduce the errors arising from the sandstone specimen heterogeneity. Consequently, two segments of a fractured specimen were processed as $\Phi 50 \times 100$ -mm cylindrical specimens for the uniaxial and conventional triaxial tests, and two cylindrical specimens with a diameter of 50 mm and a length of 30 to 35 mm were processed for the tensile test. The physical and mechanical parameters of the specimens were then tested in saturation to further explore variation regularity.

In the process of soaking, sandstone specimens were kept in a sealed environment to avoid interference from external factors. Figure 4 shows the WDT-1500 multifunctional material testing machine (Tinius Olsen, USA) used for the experiment.

To remove possible errors resulting from the inhomogeneity of the rock and to ensure comparability of test results, the same sandstone specimens were used for the P-wave velocity test and for observing the sandstone specimens' surfaces.

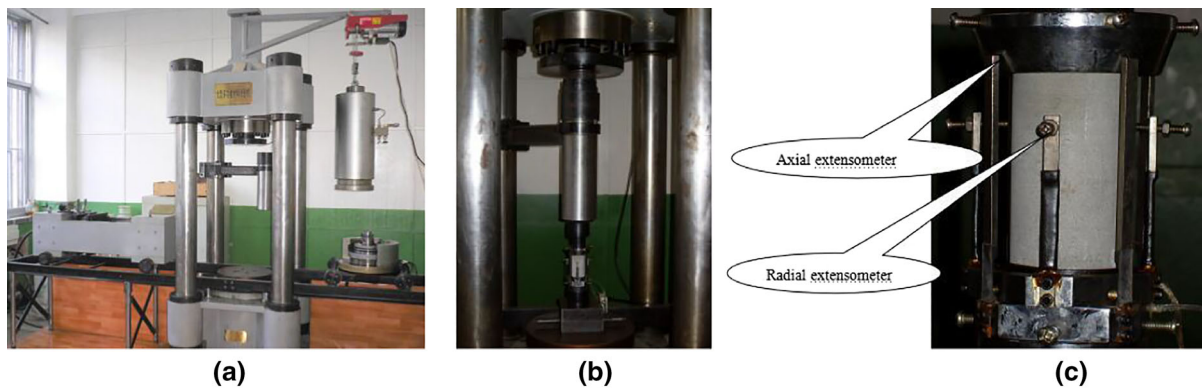


Figure 4

Experiment equipment. **a** WDT-1500 universal testing machine. **b** Installation of sample. **c** Extensometer

3. Test Results and Discussion

3.1. Porosity and P-Wave Velocity Analysis

The porosity of the specimens was determined by indirect measurement (Han et al. 2015, 2018) under various chemical solutions. As shown in Fig. 5, the porosity gradually increased with the increase in chemical immersion duration, but the specimens' P-wave velocities gradually decreased.

In the initial stage (0–1 month), the lower the pH in the solutions, the greater the porosity and the reduction of the P-wave velocities of the specimens; that is, the increases in porosity and reduction in P-wave velocity in the Na_2SO_4 (pH = 12.0) solution were less than those in the Na_2SO_4 (pH = 7.0) and

Na_2SO_4 (pH = 3.0) solutions, being the greatest in the Na_2SO_4 (pH = 3.0) solution. As the chemical immersion time increased (2–5 months), the deterioration degree of porosity and P-wave velocity in the Na_2SO_4 (pH = 12.0) solution gradually increased, but were still less than those in the Na_2SO_4 (pH = 3.0) solution and greater than those in the Na_2SO_4 (pH = 7.0) solution.

During the first month, the porosity of the specimens increased. Meanwhile, the internal flaws of the sandstone were filled with chemical solutions under the effect of the water–rock interaction. As a result, the homogeneity of the specimens improved, resulting in an increased P-wave velocity. The homogeneity of the chemical solution concentration inside the specimens might have been improved if the

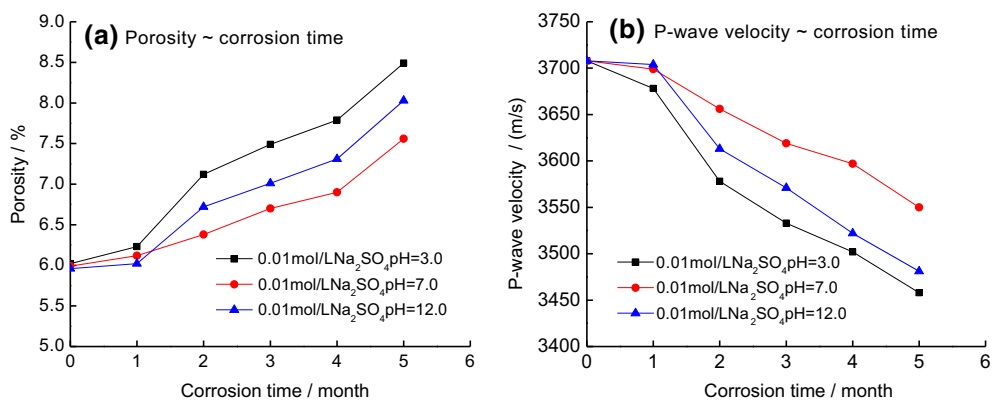


Figure 5

The relationship among porosity, P-wave velocity of sandstone, and chemical corrosion time under different chemical solutions

specimens had high porosity, which could cause the P-wave velocity to significantly increase. Thereafter, with the increase in chemical soaking time, the change rates of porosity and P-wave velocity increased; that is, the porosity increased with an increase in chemical soaking time, and the P-wave velocity showed the opposite trend.

3.2. Analysis of Fracture Toughness (K_{IC}), Tensile Strength, and Mechanical Parameters Under Uniaxial Compression Testing

The stress–strain curves of the sandstone specimens all underwent dense pore pressure, linear elastic, yield, and failure stages. As can be seen in Fig. 6, the “soft” trend of the stress–strain curves of specimens was more obvious in the various chemical solutions than that of specimens in the natural state.

- The compaction stage of the specimens was not obvious or brief under the natural condition, resulting in the deformation turning into the elastic deformation stage earlier. But the duration of the compaction stage increased to varying degrees in different chemical solutions. This duration was related to the development of pore fissures inside the specimens. Due to the increase in the porosity of the specimens immersed in the chemical solutions, the compaction stage was more and more obvious, and the nonlinearity of the curves increased.
- The elastic modulus of the specimens immersed in different chemical solutions was inferior to that of specimens under a natural state, reflecting

the degree of damage from the chemical solutions. Meanwhile, the yield stress of the specimens decreased in the solutions. Therefore, the specimens reached the yield stage earlier, which caused the elastic stage to become shorter and the yield stage to lengthen.

- The yield stage of the stress–strain curves was not obvious under the natural state, whereas the yield stage of the specimens exposed to different chemical solutions increased to varying degrees. With an increasing chemical soaking time, the yield stage became more and more obvious. The peak strain of the specimens immersed in chemical solutions was greater than that under the natural state. This was mainly due to the softening effect of the chemical solutions on the specimens; the greater the softening effect of the chemical solutions, the larger the peak strain of the specimens.
- The stress–strain curves of the specimens reached the destruction stage after the peak period. The strain rapidly increased, whereas the stress of the specimens greatly decreased. The brittleness of the specimens was remarkable when its damage occurred under the natural state, being accompanied by an obvious cracking sound. However, the brittleness of specimens soaked in chemical solutions was less pronounced.

As seen in Fig. 7, the fracture toughness K_{IC} , uniaxial compressive strength, and tensile strength of the sandstone specimens soaked in chemical solutions were lower than those in a natural state. As the chemical soaking time increased, the degree of

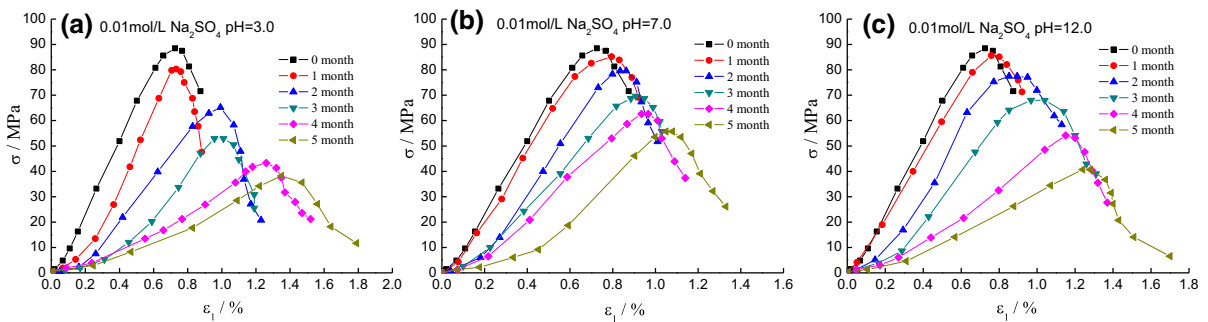


Figure 6

The stress–strain curves of sandstone specimens eroded in different chemical solutions under uniaxial compression

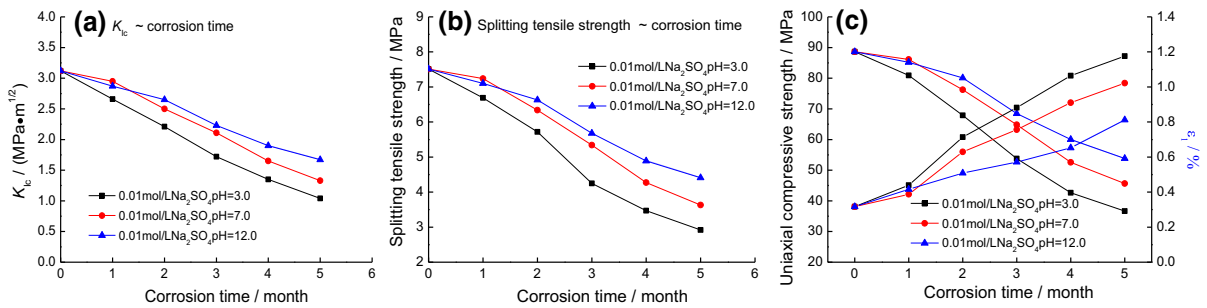


Figure 7

The relationship among K_{Ic} , splitting tensile strength, uniaxial compressive strength, and its peak strain of sandstone and chemical corrosion time under different chemical solutions

chemical deterioration gradually increased. Meanwhile, K_{Ic} , uniaxial compressive strength, and tensile strength varied in degree of deterioration under different chemical solutions.

In the initial stage (0–1 month), K_{Ic} , uniaxial compressive strength, and tensile strength of sandstone soaked in the Na_2SO_4 (pH = 3.0) solutions were less than those in the Na_2SO_4 (pH = 7.0) and Na_2SO_4 (pH = 12.0) solutions; and those of sandstone specimens in Na_2SO_4 (pH = 12.0) were the greatest. Within 2 to 5 months, the deterioration of mechanical parameters in Na_2SO_4 (pH = 12.0) gradually increased as the chemical soaking time increased and was greater than that in the Na_2SO_4 (pH = 7.0) solutions, but still less than that in the acidic Na_2SO_4 (pH = 3.0) solutions. Therefore, there was a threshold value of between 1 and 2 months for changes to occur in the fracture toughness, uniaxial compressive strength, and tensile strength of sandstone specimens in the Na_2SO_4 (pH = 12.0) solution.

As can be seen from Fig. 7c, compared with the peak strain of sandstone specimens under natural state, the peak strain significantly increased under chemical solutions. With an increase in chemical soaking time, the peak strain gradually increased. In the initial stage (0–1 month), the peak strain of specimens in Na_2SO_4 (pH = 3.0) solutions was greater than that in Na_2SO_4 (pH = 7.0) and Na_2SO_4 (pH = 12.0) solutions, with the lowest peak strain being in Na_2SO_4 (pH = 12.0) solutions. Within 2 to 5 months, the peak strain of specimens in Na_2SO_4 (pH = 12.0) solutions significantly increased; that is, $\epsilon_{1, \text{pH}=3} > \epsilon_{1, \text{pH}=12} > \epsilon_{1, \text{pH}=7}$.

3.3. Analysis of Stress–Strain Curves and Mechanical Parameters Under Conventional Triaxial Testing

The $(\sigma_1 \sim \sigma_3) \sim \epsilon_1$ curves of the sandstone specimens under the triaxial condition were the same as those under the uniaxial condition, and specimens also underwent dense pore pressure, linear elastic, yield, and failure stages.

As can be seen from Figs. 8, 9, 10, 11, and 12, the original defects and the increased pores after corrosion in the specimens were compacted under a certain initial axial pressure and confining pressure, which resulted in the compaction stage of the $(\sigma_1 \sim \sigma_3) \sim \epsilon_1$ curves not being evident under the triaxial test. It was clearly observed from Figs. 9, 10, 11, and 12 that the higher the confining pressure, the greater the initial stress on the specimens, and the denser the internal defects of the specimens will be. This resulted in the compaction stage of the $(\sigma_1 \sim \sigma_3) \sim$

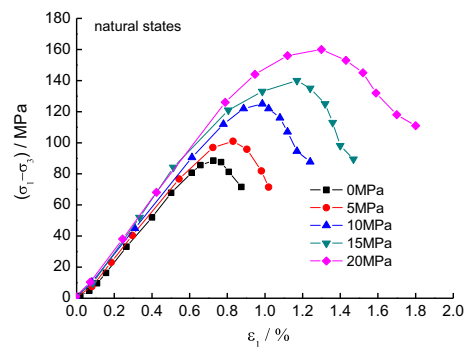


Figure 8

The $(\sigma_1 - \sigma_3) \sim \epsilon_1$ curves of sandstone specimens under natural state and triaxial compression

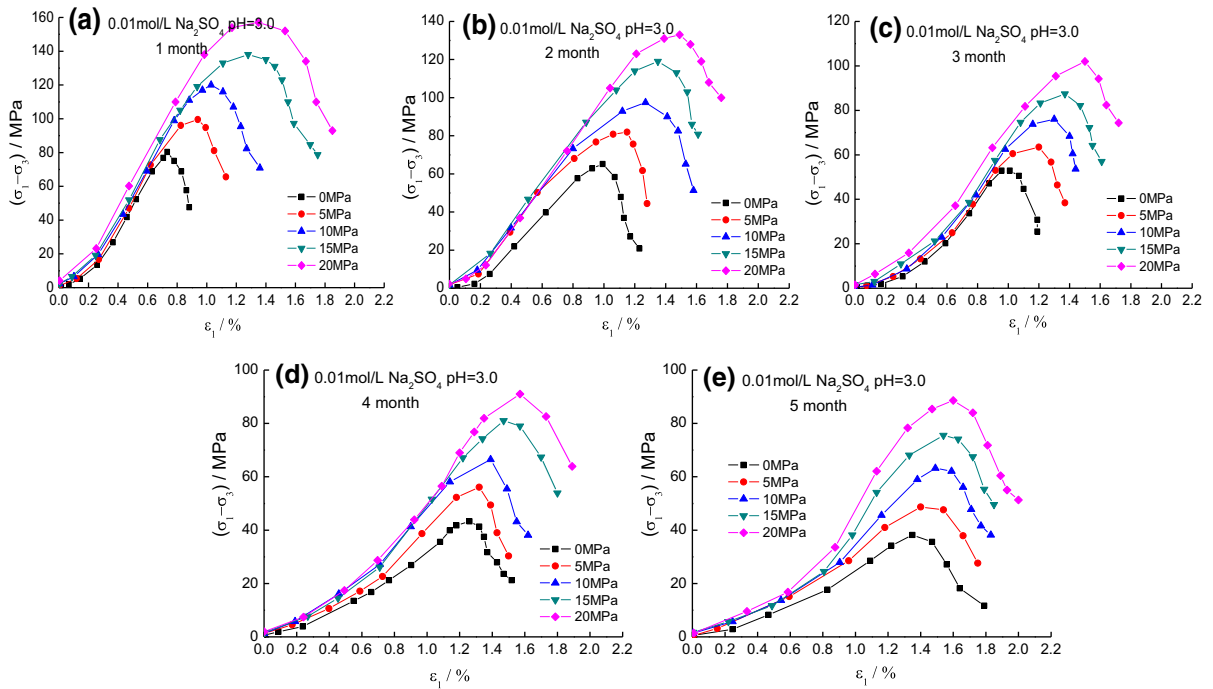


Figure 9

The $(\sigma_1 - \sigma_3) \sim \varepsilon_1$ curves of sandstone specimens eroded in 0.01 mol/L Na_2SO_4 pH = 3.0 solutions under triaxial compression

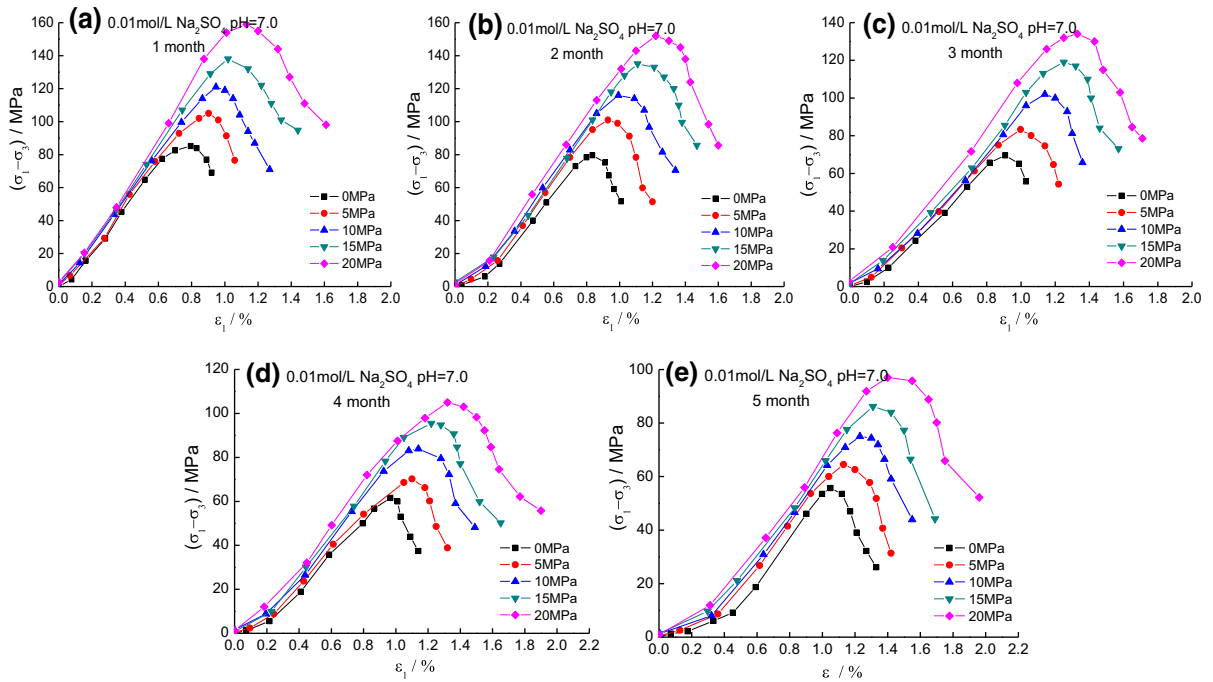


Figure 10

The $(\sigma_1 - \sigma_3) \sim \varepsilon_1$ curves of sandstone specimens eroded in 0.01 mol/L Na_2SO_4 pH = 7.0 solutions under triaxial compression

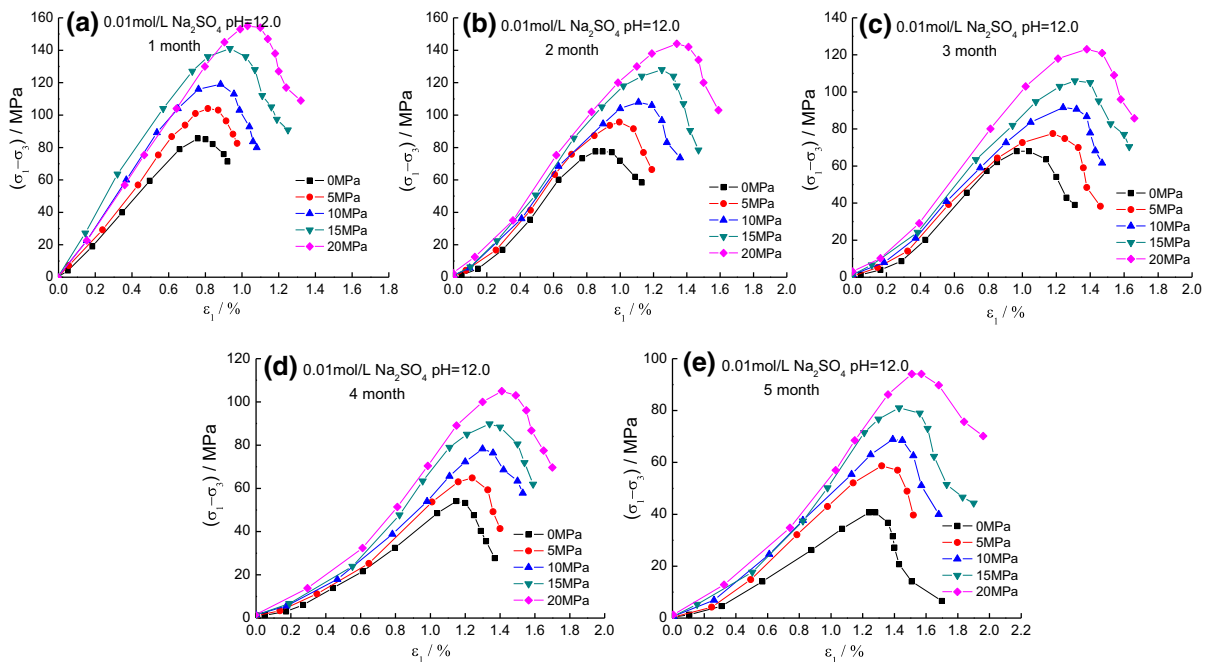


Figure 11

The $(\sigma_1 - \sigma_3) \sim \varepsilon_1$ curves of sandstone specimens eroded in 0.01 mol/L Na_2SO_4 pH = 12.0 solutions under triaxial compression

ε_1 curves of the specimens not being evident and led the specimens into the elastic stage. Meanwhile, the stiffness (elastic modulus) of the specimens also gradually increased with the increase of confining pressure. As mentioned above, the higher the softening degree of the specimens exposed to chemical solutions, the smaller the elastic modulus. The yield stress of specimens exposed to different chemical solutions increased to varying degrees than that under the natural state. Therefore, the specimens reached the yield stage earlier, which caused the elastic stage to become shorter and the yield stage to lengthen. Moreover, with increasing chemical soaking time and confining pressure, the plastic property became more and more obvious. Meanwhile, the brittleness of specimens soaked in chemical solutions reduced; however, the ductile and failure characteristics of the specimens gradually increased with increasing chemical soaking time or confining pressure.

Figures 9, 10, 11, and 12 showed that the peak strength and peak strain of specimens in chemical solutions significantly increased with increases in confining pressure or chemical soaking time, which were greater than the peak strength and peak strain of

specimens under uniaxial compression. There was a marked difference in the peak strengths and peak strains of specimens immersed in different chemical solutions. Under the same confining pressure, the peak strength in the natural state was greater than that of specimens immersed in chemical solutions, but this result was reversed for peak strain.

Under the same confining pressure, the peak strain of specimens immersed in chemical solutions gradually increased with an increase in corrosion time. For the 0 to 1-month period, the peak strains of sandstone specimens in Na_2SO_4 (pH = 3.0) solutions were greater than those in Na_2SO_4 (pH = 7.0) and Na_2SO_4 (pH = 12.0) solutions under the same confining pressure, with the lowest peak strain being in Na_2SO_4 (pH = 12.0) solutions. Within 2 to 5 months, the peak strain followed the sequence $\varepsilon_{1, \text{pH}=3} > \varepsilon_{1, \text{pH}=12} > \varepsilon_{1, \text{pH}=7} > \varepsilon_{1, \text{natural}}$.

The cohesions and internal friction angles of the specimens in different chemical solutions are shown in Fig. 13. Figure 13 shows that the cohesive strengths and internal friction angles in the natural state were greater than those of specimens immersed in chemical solutions. The cohesive strengths and

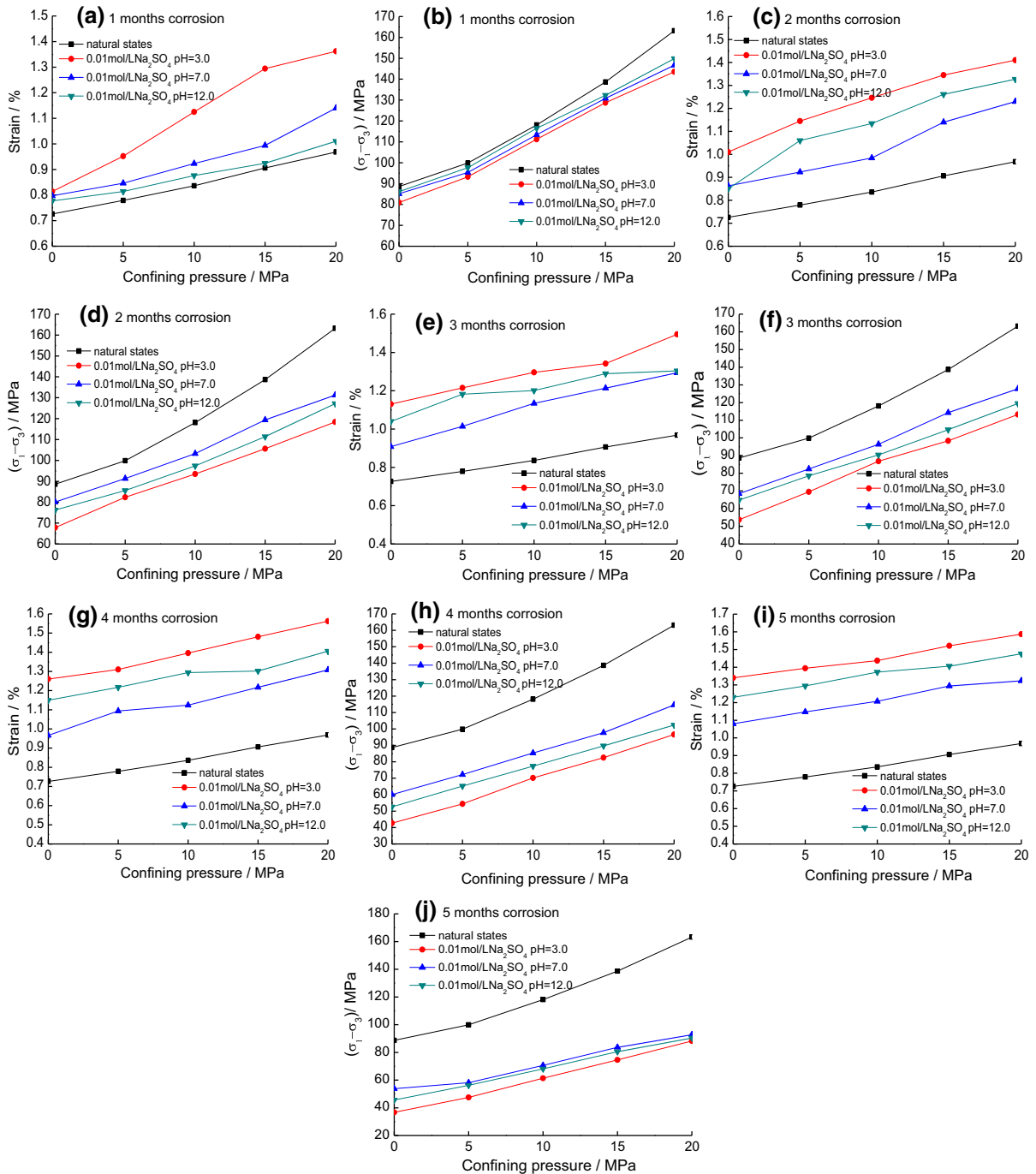


Figure 12

The relationships among peak strength, peak strain, and confining pressure of sandstone specimens under different chemical solutions

internal friction angles gradually decreased with an increase in chemical soaking time. However, there were differences in the decreases of the cohesive

strengths and internal friction angles for sandstone specimens immersed in different chemical solutions. For the 0 to 1-month period, the cohesive strengths

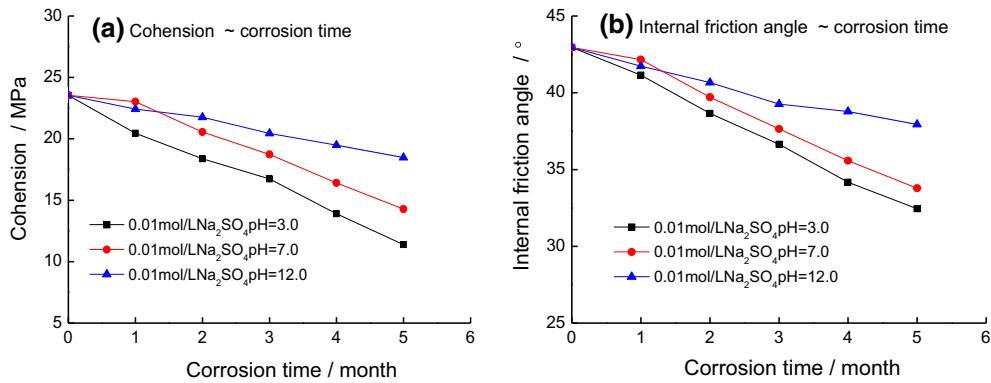


Figure 13

The relationship among cohesion, internal friction angle of sandstone, and chemical corrosion time under different chemical solutions

and internal friction angles in Na₂SO₄ (pH = 3.0) solutions were less than those in Na₂SO₄ (pH = 7.0) and Na₂SO₄ (pH = 12.0) solutions, with the lowest being in Na₂SO₄ (pH = 12.0) solutions. Within 2 to 5 months, the deterioration degree of the cohesion strength and internal friction angle in acidic Na₂SO₄ (pH = 3.0) was the greatest followed by that of the specimens in Na₂SO₄ (pH = 7.0) and Na₂SO₄ (pH = 12.0), with that in Na₂SO₄ (pH = 7.0) being relatively small. That is, cohesion strength and internal friction angle of the specimens followed the sequence $c_{pH=7} > c_{pH=12} > c_{pH=3}$ and $\varphi_{pH=7} > \varphi_{pH=12} > \varphi_{pH=3}$.

3.4. Analysis of the Correlation of Mechanical Parameters

The relations among the cohesion, internal friction angle, splitting tensile strength, uniaxial compressive strength of sandstone, and the K_{Ic} value of sandstone were evaluated, as shown in Fig. 14. As can be seen, there was a linear relation among cohesion, internal friction angle, tensile strength, uniaxial compressive strength, and fracture toughness K_{Ic} of the sandstone specimens.

A linear regression analysis of the relation between the mechanical parameters of the specimens and the fracture toughness K_{Ic} was done (Fig. 14); the relations can be expressed by Eqs. (1), (2), (3), and (4):

$$\sigma = 25.6K_{Ic} + 10.671, \quad R^2 = 0.9956, \quad (1)$$

$$\sigma_t = 2.2609K_{Ic} + 0.5696, \quad R^2 = 0.9937, \quad (2)$$

$$c = 10.608 \ln(K_{Ic}) + 11.28, \quad R^2 = 0.9562, \quad (3)$$

$$\phi = 9.7387 \ln(K_{Ic}) + 31.499, \quad R^2 = 0.9623, \quad (4)$$

where σ_t , σ , and c refer to the tensile strength, uniaxial compressive strength, and cohesion of sandstone specimens, respectively (in megapascals), ϕ is the internal friction angle of the sandstone (in °), and R^2 is the correlation coefficient.

To obtain a further understanding of the damage to mechanical parameters of the sandstone exposed to chemical solutions, the chemical damage factor K_{cf} was defined as

$$K_{cf} = \frac{f_0 - f_i}{f_0}, \quad (5)$$

where f_0 and f_i are the mechanical parameters of the sandstone specimens in their natural states and after having i months of chemical soaking time, respectively (in megapascals). K_{cf} is related to the degree of chemical damage to the sandstone specimens. The value of K_{cf} is related to the resistance of sandstone specimens to chemical damage. The larger the value of K_{cf} , the greater the degree of resistance to chemical damage.

Figure 15 shows the relations among the deterioration rates of mechanical parameters and chemical damage times under different chemical solutions. Figure 15 shows that the deterioration rates of

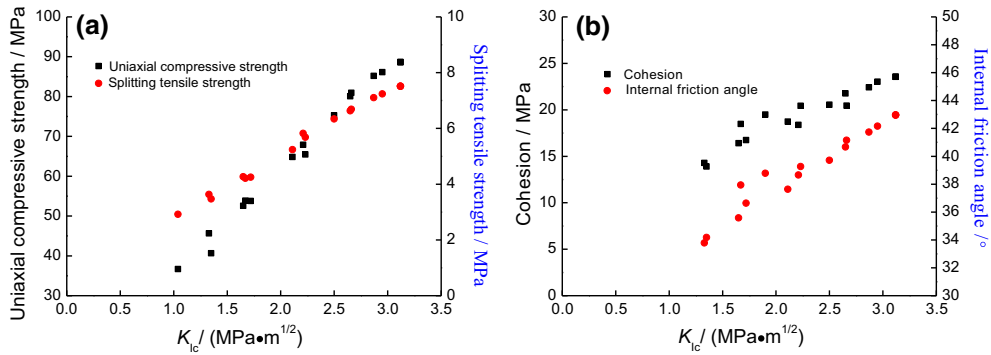


Figure 14

The relationship among K_{Ic} , cohesion, internal friction angle, splitting tensile strength, and uniaxial compressive strength of sandstone

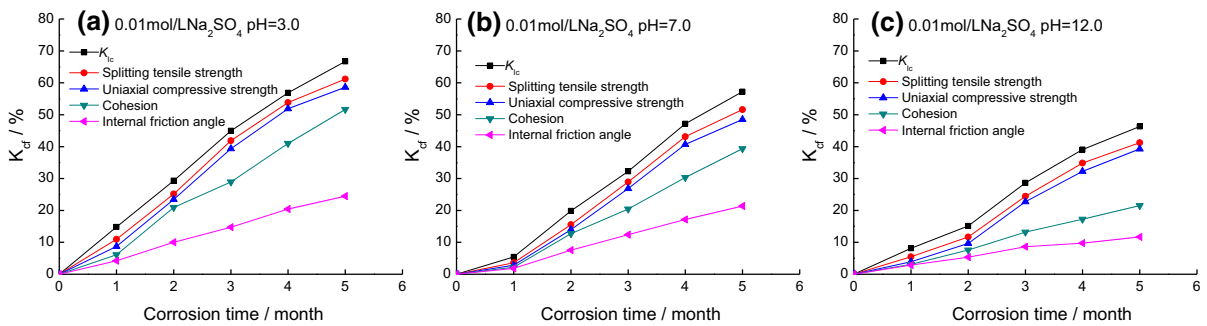


Figure 15

The relationship between deterioration rate of mechanical characteristics of sandstone and chemical corrosion time under different chemical solutions

specimens were basically consistent in different chemical solutions. Under the same corrosion time and chemical solution, the deterioration degree of the fracture toughness K_{Ic} was greater than that of other mechanical parameters, and the internal friction angle was the lowest: $K_{cf, K_{Ic}} > K_{cf, \sigma_t} > K_{cf, \sigma} > K_{cf, c} > K_{cf, \phi}$. This shows that the fracture toughness K_{Ic} of sandstone was more sensitive to chemical damage than it was to other mechanical characteristics.

The crack propagation radius r of the sandstone specimens was developed in the literature (Deng et al. 2012) under different chemical solutions. This was to describe and discuss the mechanism and reason for the fracture toughness being more sensitive to chemical solutions. The relation between the crack propagation radius of sandstone and the chemical

corrosion time under different chemical solutions is shown in Fig. 16.

$$r = \frac{1}{2\pi} \left(\frac{K_{Ic}}{\sigma_t} \right)^2, \tag{6}$$

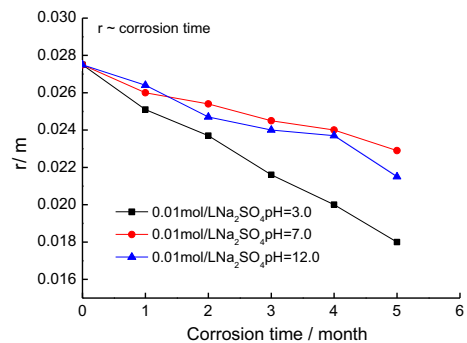


Figure 16

The relationship between crack propagation radius, r of sandstone, and chemical corrosion time under different chemical solutions

where r is the crack propagation radii (m). Previous research results show that the crack propagation radius gradually increases with increasing rock strength.

As can be seen in Fig. 16, the crack propagation radius r under various chemical solutions decreased to varying degrees more than that of the sandstone specimens under the natural state, and generally decreased with the increase in chemical corrosion time. This indirectly indicates that the mechanical parameters of the sandstone had different degrees of degradation depending on the chemical corrosion time.

Equation (6) indicates that both the tensile strength and the crack propagation radius of the sandstone were reduced at the same time. Compared with the deterioration degree of the tensile strength and compressive strength of the sandstones, that of the fracture toughness K_{Ic} was significantly higher under various chemical solutions. This was consistent with the test results shown in Fig. 15, which show that the deterioration degree of the fracture toughness K_{Ic} was the highest, followed by that of tensile strength, and the compressive strength was relatively low.

A crack in brittle materials such as rocks is generally an open-mode crack. When the stress intensity factor at the crack tip reaches the fracture toughness K_{Ic} , the crack will rapidly expand. When the stress intensity factor at the crack tip is less than the fracture toughness K_{Ic} , the crack growth rate will continuously increase, but the crack growth is stable at this time, which is called stress corrosion subcritical crack growth (Zhang et al. 1981).

The attenuation of fracture toughness was clear for sandstone specimens corroded by a hydrochemical solution, and the weakening effect gradually increased with increasing corrosion time. A series of complex physical and chemical reactions occurred between the sandstone and the chemical solutions. These reactions caused varying degrees of damage to the sandstone microstructure, such as increasing porosity and mineral particle deterioration, which loosened the specimens. As a result, the specimens' internal stress fields caused an uneven distribution of stresses and stress concentrations due to the differences in deformation characteristics and force

transfer rates. These led to microcrack initiation in the tips of the prefabricated cracks: this showed that the weakening effect depends on the soaking time. The weakening effect of sandstone accelerates the subcritical crack growth of rocks under the action of water chemical corrosion (Wang et al. 2011).

4. Analysis of the Damage Variable Mechanism

4.1. Regularities in the Variations of Physical Properties

The concentrations of Ca^{2+} and Mg^{2+} ions dissolved in different chemical solutions were measured each month during the chemical soaking time, as shown in Fig. 17. The concentrations of Ca^{2+} and Mg^{2+} ions dissolved in the solutions gradually increased as the chemical immersion time increased. However, the ion concentrations varied as deterioration occurred in the different chemical solutions.

In the first month, the concentrations of Ca^{2+} and Mg^{2+} ions dissolved in the Na_2SO_4 (pH = 3.0) solution were greater than that in the Na_2SO_4 (pH = 7.0) and Na_2SO_4 (pH = 12.0) solutions, with the lowest concentration being in the Na_2SO_4 (pH = 12.0) solution. As the chemical soaking time increased (2–5 months), the concentrations of Ca^{2+} and Mg^{2+} ions dissolved in the Na_2SO_4 (pH = 12.0) solution gradually increased, but were still lower than those in the Na_2SO_4 (pH = 3.0) solution and higher than those in the Na_2SO_4 (pH = 7.0) solution.

4.2. Damage Variable

The damage variable D is expressed as

$$D = \frac{n_{(it)} - n_{(i0)}}{1 - n_{(i0)}} = 1 - \frac{1 - n_{(it)}}{1 - n_{(i0)}}, \quad (7)$$

where $n_{(i0)}$ refers to the porosity of saturated sandstone specimens under the natural state, and $n_{(it)}$ is the porosity of saturated sandstone specimens after i months of chemical soaking time.

Figure 18 shows the relations between the damage variables and the chemical soaking times in various chemical solutions. The damage to specimens

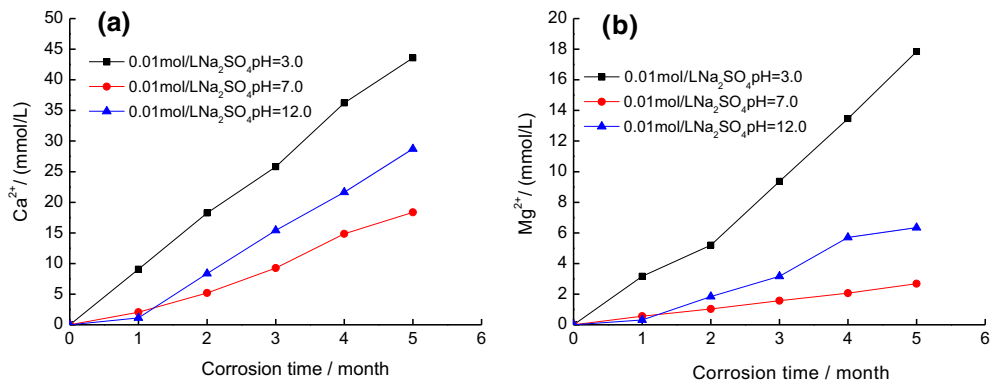


Figure 17

The relationship between Ca^{2+} and Mg^{2+} of different chemical solutions and chemical corrosion time

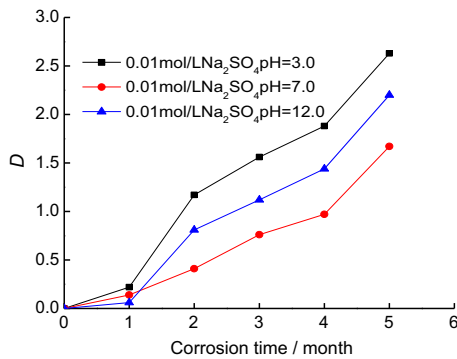


Figure 18

The relationship between damage variable of sandstone and chemical corrosion time under different chemical solutions

increased to different degrees in the chemical solutions and gradually increased with an increase in chemical soaking time. A certain distinction existed in the variation regularity of the degree of damage from different chemical solutions.

During the first month, the degree of chemical damage to the specimens was higher in acidic Na_2SO_4 (pH = 3.0) solutions than that in Na_2SO_4 (pH = 7.0) and alkaline Na_2SO_4 (pH = 12.0) solutions. The degree of chemical damage in alkaline Na_2SO_4 (pH = 12.0) solutions was the lowest; that is, $D_{\text{pH}=3.0} > D_{\text{pH}=7.0} > D_{\text{pH}=12.0}$. However, with an increase in chemical soaking time, the damage degree to specimens in the Na_2SO_4 (pH = 12.0) solution gradually increased, but was still less than that in the Na_2SO_4 (pH = 3.0) solution and greater than that in

Na_2SO_4 (pH = 7.0) solution; that is, $D_{\text{pH}=3.0} > D_{\text{pH}=12.0} > D_{\text{pH}=7.0}$.

4.3. Effects of Damage on Physical and Mechanical Parameters

Figure 19 shows the relations between the physical mechanical parameters of the sandstone specimens and the damage variables in different chemical solutions based on a statistical analysis of the experimental results.

As seen in Fig. 19, the physical mechanical parameters of specimens affected by chemical solutions gradually deteriorated as the degree of chemical damage increased. That is, the chemical solutions led the microstructures of the specimens to deteriorate. The deterioration gradually increased with the increase in chemical soaking time. The chemical damage accumulated and might have resulted in varying degrees of deterioration of the physical mechanical parameters.

The regression analysis was done on the results shown in Fig. 19. The relations between the physical mechanical parameters of the sandstone and the damage variables were obtained as follows:

$$K_{\text{Ic}} = 3.089e^{-0.398D}, \quad R^2 = 0.9651 \quad (8)$$

$$\sigma_t = 7.5476e^{-0.353D}, \quad R^2 = 0.9553 \quad (9)$$

$$\sigma = 89.63e^{-0.331D}, \quad R^2 = 0.9565 \quad (10)$$

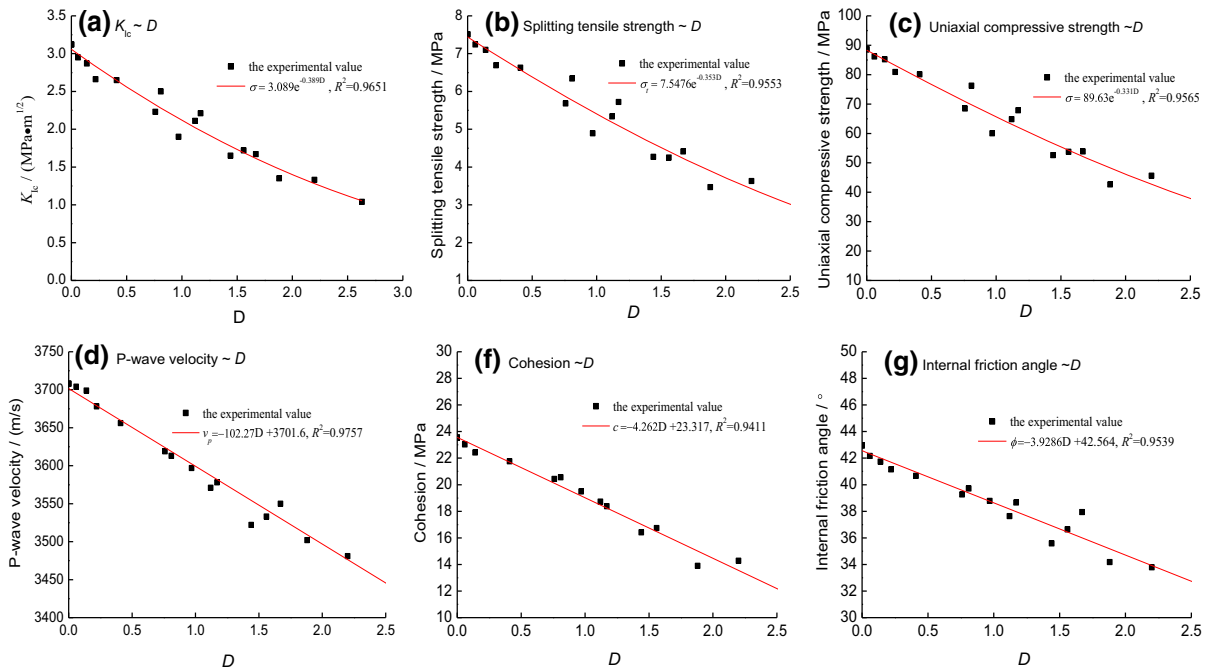


Figure 19

The relationship between physical mechanical parameters of sandstone and damage variable under different chemical solutions

$$c = -4.2625D + 23.317, \quad R^2 = 0.9411 \quad (11)$$

$$\phi = -3.9286D + 42.564, \quad R^2 = 0.9539 \quad (12)$$

$$v_p = -102.27D + 3701.6, \quad R^2 = 0.9757 \quad (13)$$

$$D = 0.061(Ca^{2+}) + 0.0733, \quad R^2 = 0.9295 \quad (14)$$

$$D = 0.1379(Mg^{2+}) + 0.2644, \quad R^2 = 0.9072 \quad (15)$$

A linear regression analysis was done on the results shown in Fig. 20. The relations between the Ca^{2+} and Mg^{2+} ions dissolved in chemical solutions and the damage variables were obtained as

4.4. Effects of the Ion Concentration on the Physical and Mechanical Parameters

The relations between the physical and mechanical parameters of sandstone specimens and ion concentration dissolved in chemical solutions are shown in Fig. 21.

As seen in Fig. 21, there were clear consistencies in the relations among the degree of damage to mechanical parameters, physical parameters, and ion concentrations dissolved in the chemical solutions. During the process of chemical damage, the greater the concentrations of Ca^{2+} and Mg^{2+} ions dissolved in a solution, the greater the deterioration degree of physical mechanical parameters.

By substituting Eqs. (14) and (15) into Eqs. (8) and (13), the correlation relations among physical and mechanical parameters of sandstone, damage

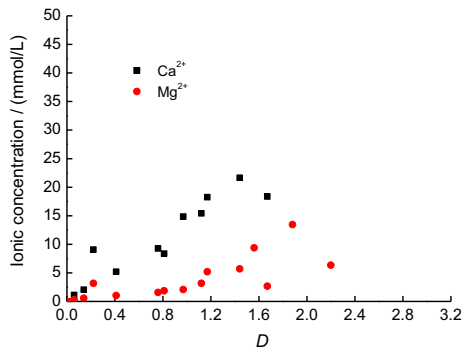


Figure 20

The relationship between Ca^{2+} , Mg^{2+} ion concentration, and damage variable

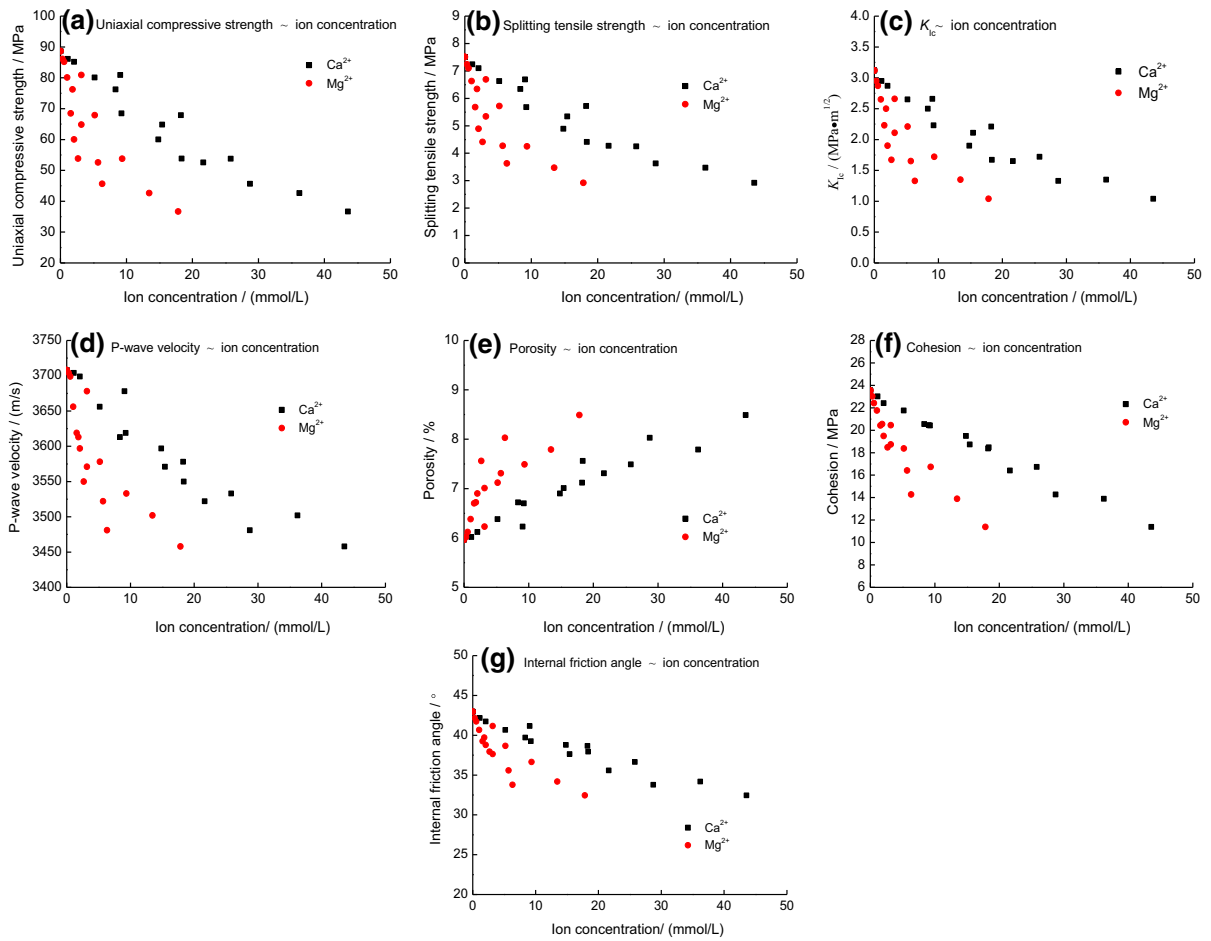


Figure 21

The relationship among the damage degree of physical and mechanical properties and Ca^{2+} and Mg^{2+} ions concentration dissolved in the corresponding chemical solution

variables, and ion concentrations of calcium and magnesium were obtained.

4.5. Microstructural Characteristics of Sandstone

The surface microstructure of specimens immersed in chemical solutions was observed using an XTL-100E stereomicroscope. Figures 22 and 23 show scanning electron microscopy (SEM) images of the internal microstructure of specimens after 5 months of chemical soaking time in different chemical solutions.

As can be seen from Fig. 22, there was an absence of pitting corrosion and holes on the surfaces of the sandstone, and the surface mineral particles were

relatively large with sharp edges and corners. However, the surfaces were seriously degraded by corrosion in different chemicals; for example, there were varying degrees of pitting corrosion and holes. In addition, the sizes of the holes and the degrees of pitting corrosion gradually increased with an increase in chemical soaking time, and the damage degree to microstructures on the surfaces of the specimens gradually increased. However, the damage degrees to sandstones immersed in different chemical solutions varied.

During the first month, there was a greater degree of hole and pit corrosion damage to the surfaces of sandstone immersed in the acidic Na_2SO_4 (pH = 3.0) solution, but there was no evident change for

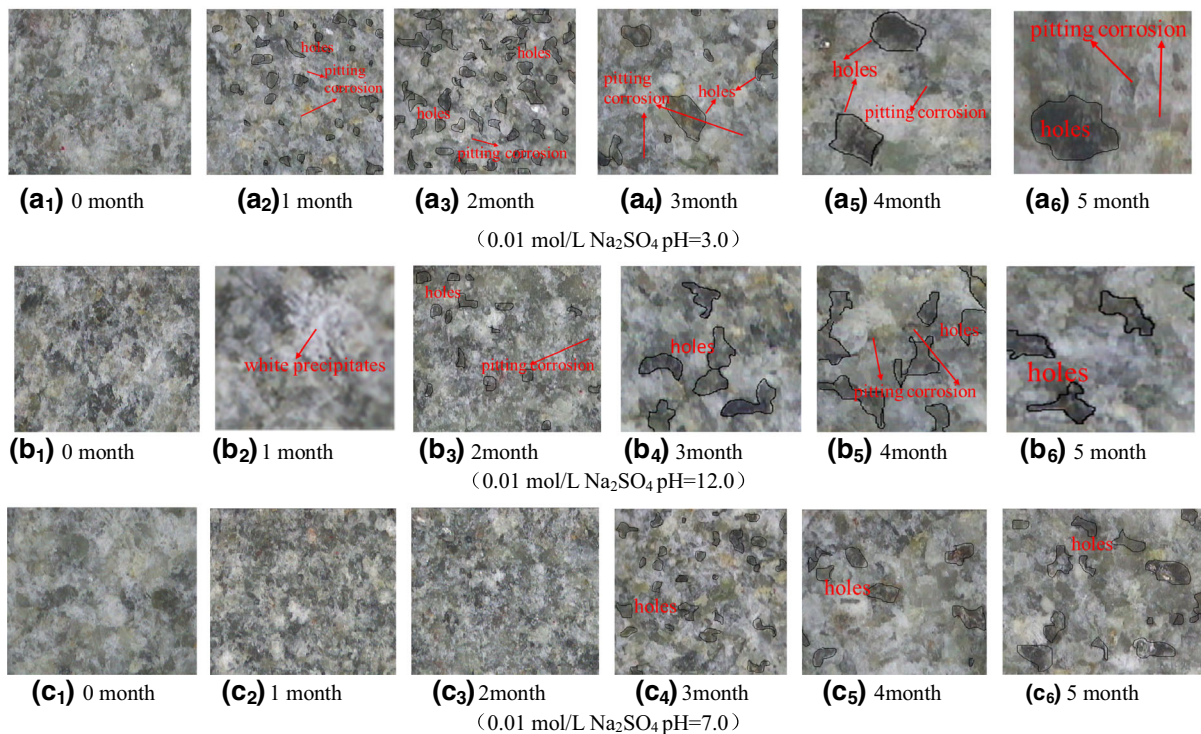


Figure 22
Photos of surface microstructure of sandstone specimens under different chemical solutions

specimens immersed in the Na_2SO_4 ($\text{pH} = 7.0$) or Na_2SO_4 ($\text{pH} = 12.0$) solution. Meanwhile, many white precipitates were deposited on the surface of specimens immersed in the Na_2SO_4 ($\text{pH} = 12.0$) solution. The possible cause was the main ingredients, $\text{Ca}(\text{OH})_2$ and $\text{Mg}(\text{OH})_2$, which hindered the percolation of chemical solutions into the interior of the specimens and inhibited chemical damage to the sandstone specimens. Meanwhile, the consumption of H^+ in the solution gradually decreased through chemical reactions between the water and the rock, which caused the chemical solutions to become weakly alkaline. The alkaline environment was conducive to the precipitation of these white precipitates, which exacerbated the hindrance effect. This indirectly showed that the alkaline chemical solution had a certain protective effect on the specimens.

Later, the white precipitation gradually disappeared until 2 months of chemical soaking time, and the size of holes and the degree of pitting corrosion on the surfaces of the sandstone gradually increased.

This may explain why the damage of specimens in the Na_2SO_4 ($\text{pH} = 7.0$) solution was greater than that in the alkaline Na_2SO_4 ($\text{pH} = 12.0$) solution. Later, the white precipitate gradually disappeared as the chemical soaking time increased (2–5 months), and holes and pitting corrosion increased on the surfaces of the specimens. However, the degree of chemical damage on the surfaces of specimens in the Na_2SO_4 ($\text{pH} = 12.0$) solution was still less than that in the acidic Na_2SO_4 ($\text{pH} = 3.0$) solution and greater than that in the Na_2SO_4 ($\text{pH} = 7.0$) solution.

As can be seen in Fig. 23, there were varying degrees of internal corrosion degradation of the samples as they suffered the effects of the chemical solutions. The internal morphology of the sandstone specimens was relatively coarse in its natural state. The main component was SiO_2 , as found from the energy dispersion spectrum obtained by SEM; the mineral particles were relatively large, the edges and corners of the mineral grains were very clear, and the structure of the internal morphology was dense.

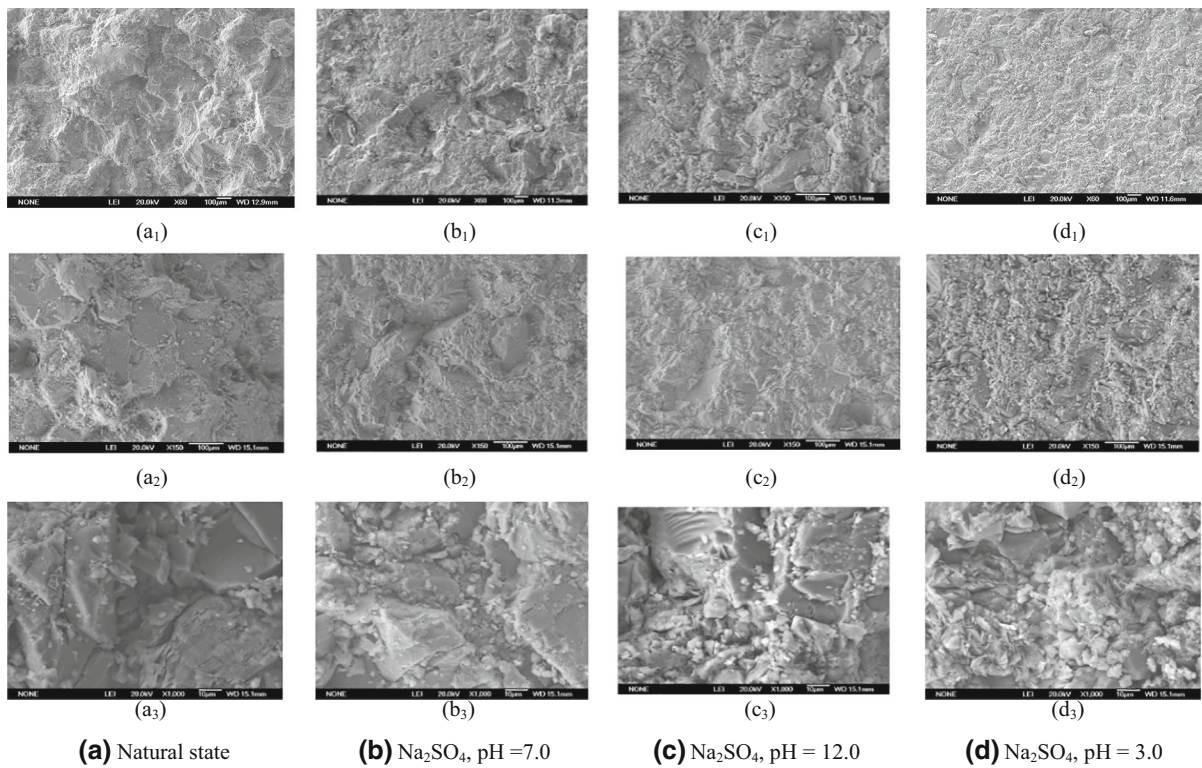


Figure 23

SEM images of sandstone specimens under different chemical solutions after 5 months of corrosion

However, in our specimens, many small mineral particles were generated in the rock under the effects of various chemical solutions, and the edges and corners of the mineral grains gradually disappeared or became smoother, while the roughness of the mineral grains gradually decreased and the sandstone structure became looser.

Figure 23 shows that the particle sizes in the sandstone specimens gradually decreased under the effect of the chemical solutions compared with those in sandstone in the natural state, contributing to the fragility of their structures. There were also differences in the chemical damage to the internal microstructures of the specimens in different chemical solutions. The grain sizes of the sandstone decreased, the cementing material eroded away in the acidic Na_2SO_4 (pH = 3.0) solution, and the roundness of the sandstone grains increased. The microstructure deteriorated more when specimens were immersed in the Na_2SO_4 (pH = 7.0) and Na_2SO_4 (pH = 12.0) solutions than under natural

conditions, but the deterioration was less than for specimens immersed in the Na_2SO_4 (pH = 3.0) solution. This indicates that the acidic Na_2SO_4 (pH = 3.0) solution aggravated the chemical damage deterioration to the internal microstructure of the sandstone.

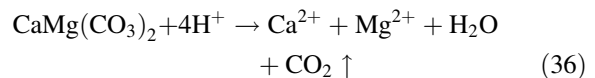
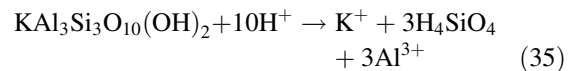
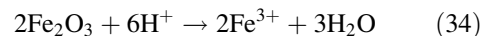
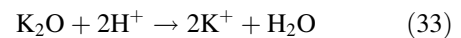
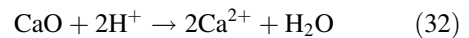
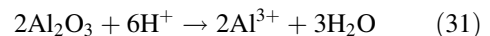
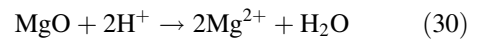
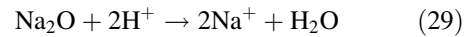
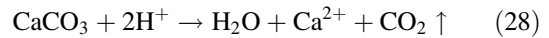
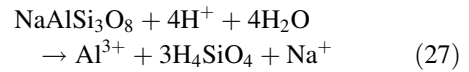
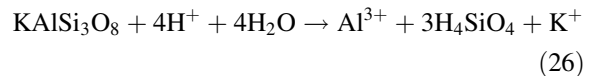
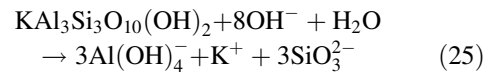
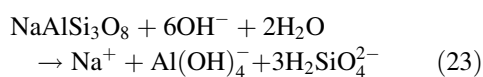
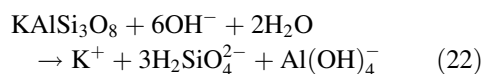
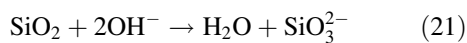
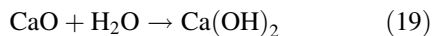
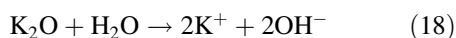
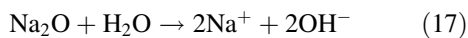
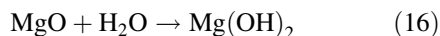
4.6. Analysis of the Damage Variable Mechanism

A series of complex physical and chemical reactions occurred between the sandstone and the chemical solutions. The reactions caused varying degrees of damage to the microstructure of the sandstone and loosened and weakened the specimens by, for example, increasing their porosity, deteriorating their mineral particles, and finally changing their mechanical characteristics and stress states. In actual engineering, many geological disasters are closely associated with the complex process of water–rock corrosion. The mineral composition of our sandstone specimens was not homogeneous. As a result, due to

differences in deformation characteristics and force transfer rates during loading, the internal stress fields of the specimens cause an uneven distribution of stresses and stress concentrations. These led to microcrack initiation in the tips of the prefabricated cracks. The interactions mentioned above all occurred at basically the same time and influenced each other.

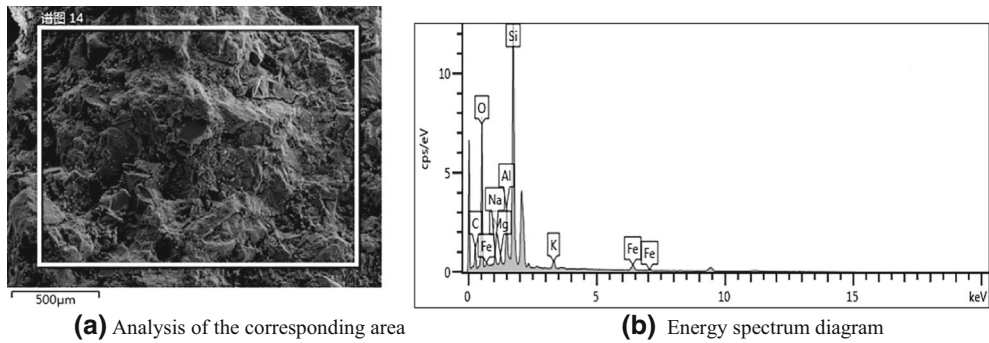
The sandstones used in the tests were identified via mineral appraisal as medium and fine calcareous quartz sandstones. The main mineral composition comprised quartz, feldspar (e.g., potassium feldspar, sodium feldspar, and calcium feldspar), small amounts of mica (biotite and white mica), and small amounts of debris and metal minerals. The type of cementation was porous cement; its main ingredient was a carbonate. The formula of quartz was SiO_2 and alkaline oxide; the formulas of potassium feldspar or potash feldspar, sodium feldspar, and calcium feldspar were KAlSi_3O_8 , $\text{NaAlSi}_3\text{O}_8$, and $\text{CaAl}_2\text{Si}_2\text{O}_7$, respectively. The formula of mica was $\text{KAl}_3\text{Si}_3\text{O}_{10}(\text{OH})_2$, and the formula of the main composition of carbonate cement was CaCO_3 . In addition, the formulas of other minerals in the sandstone, for example, Fe_2O_3 , K_2O , Al_2O_3 , and MgO , were TiO_2 , MnO , Na_2O , and CaO respectively.

There are various chemical reactions between water and rock in various chemical solutions. These are as follows:



In addition to the chemical reactions mentioned above, dissolution and hydrolytic actions took place between the water and the rock. Hydrolytic action occurred between the K^+ , Ca^{2+} , Na^+ , and Mg^{2+} of the rock minerals and the OH^- ions in the solutions and caused the minerals to dissolve and generate new minerals. The dissolution action caused the sandstone minerals to dissolve and the porosity of the rock to increase, and finally the rock became soft and weak.

When the sandstone was immersed in 0.01 mol/L Na_2SO_4 (pH = 7.0), only chemical reactions of types (16), (17), (18), (19), and (20) occurred; there were no violent chemical reactions between water and rock, and the products were poorly soluble in water; for example, H_4SiO_4 , $\text{Ca}(\text{OH})_2$, and $\text{Mg}(\text{OH})_2$. Although these reactions caused the rock to become loose, there may have been certain repair effects on the original crack fractures of the sandstone. After the chemical reaction between the K_2O and Na_2O of the sandstone and the Na_2SO_4 (pH = 7.0) solution, the K^+ and Na^+ ions of the chemical reactants migrated



Element	Wt%	Wt% Sigma	Atomic percent /%
C	6.59	0.36	12.03
O	30.85	0.26	41.27
Na	0.91	0.09	0.96
Mg	0.76	0.08	0.84
Al	8.90	0.15	7.36
Si	40.37	0.33	31.66
K	5.74	0.16	3.26
Ca	1.67	0.14	0.96
Fe	4.32	0.30	1.71
Total	100.00		100.00

(c) Table of element content

Figure 24

Energy spectrum analysis of sandstone specimens under natural state

out of the sample into solution, which caused the chemical damage to the rock to increase. However, there was little effect on the mechanical characteristics of the specimens owing to the low level of K_2O and Na_2O in the sandstone.

This led to the chemical reactions between the sandstone and the acidic Na_2SO_4 ($pH = 3.0$) solution being more severe and more varied; for example, types (26), (27), (28), (29), (30), (31), (32), (33), (34), (35), and (36). Most reaction products were in the form of ions that loosened the sandstone and increased its porosity. Therefore, the mechanical characteristics of the sandstone deteriorated with the increase in corrosion time when they were immersed in the Na_2SO_4 ($pH = 3.0$) solution.

When the sandstone was immersed in the Na_2SO_4 ($pH = 12.0$) solution, chemical reactions of only types (21), (22), (23), (24), and (25) occurred. During

the initial stages of the tests, it was more advantageous for reaction products to fill the initial pore defects of sandstone soaked in Na_2SO_4 ($pH = 12.0$) than those in Na_2SO_4 ($pH = 7.0$), which, to a certain extent, eased the chemical damage effect of Na_2SO_4 ($pH = 12.0$) on the sandstone. The degree of degradation of mechanical characteristics of specimens in the Na_2SO_4 ($pH = 12.0$) solution was less than that in the Na_2SO_4 ($pH = 7.0$) solution. However, sedimentation gradually increased with the continuous effect of chemical corrosion and expanded. This increased the porosity of the specimens and promoted infiltration of chemical solutions into them. This indicates that the chemical damage to the specimens and the degradation degree of their mechanical parameters increased in an alkaline environment.

Figures 24 and 25 show that the internal morphology of the sandstone specimens was relatively

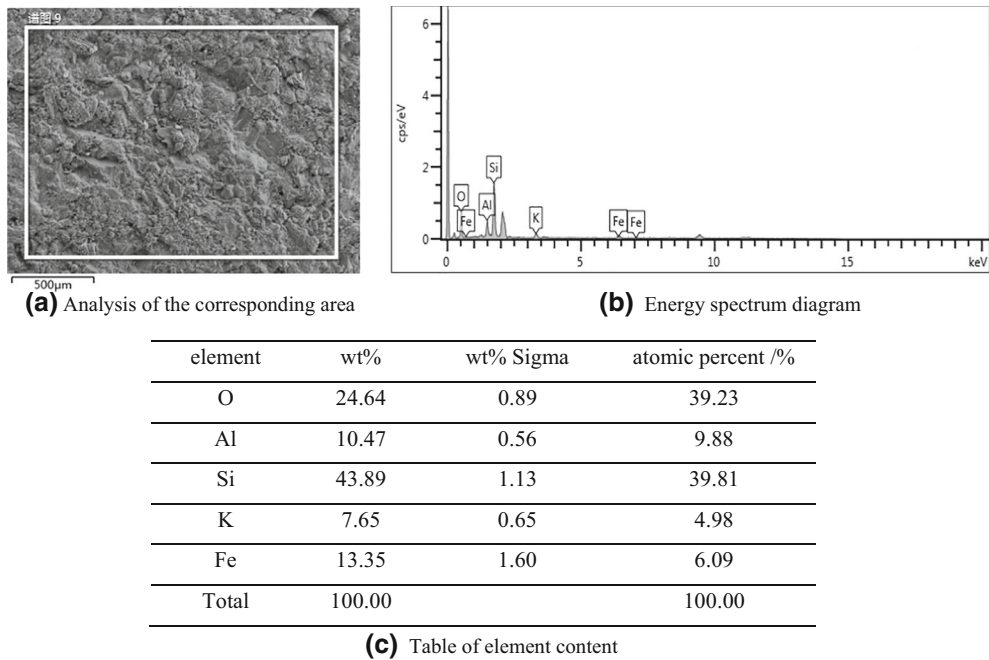


Figure 25

Energy spectrum analysis of sandstone specimens under 0.01 mol/LNa₂SO₄, pH = 3.0

coarse in its natural state, it was composed mainly of SiO₂, as found from the energy dispersion spectrum obtained by SEM, the edges and corners of the mineral grains were very clear, and the structure of the internal morphology was dense. However, there were varying degrees of internal corrosion degradation of the specimens when they suffered from the effects of various chemical solutions. Furthermore, many small mineral particles were generated in the rock under those effects; meanwhile, the edges and corners of the mineral grains gradually disappeared or became smoother, while the roughness of the mineral grains gradually decreased and the sandstone structure became looser. The calcareous cement of the sandstone samples submerged in the Na₂SO₄ (pH = 3.0) solution was found to be completely corroded. Moreover, the results of energy-dispersive X-ray spectroscopy testing show that none of the Ca²⁺ elements were present and that the amount of other elements had also decreased relative to what was typically found in the samples' natural state.

The damage to the microstructures increased the porosity and internal defects of specimens under the effect of chemical solutions. In addition, damage to

specimens gradually increased as the duration of chemical damage increased, which hindered dislocation movement during loading. The loading induced pressure on the specimens, and the pore defects closed, which further improved the sandstone microstructure. To some extent, this alleviated the deterioration of specimens under the effect of chemical solutions.

During our experiments, we found sand particles at the bottom of the vessel used for soaking the sandstone specimens. As the chemical damage duration increased, the number of sand particles gradually increased, indicating that the porosity of the sandstone increased. As the corrosion continued, the specimens changed from a relatively dense state to a loose state because of the increase in porosity.

5. Conclusions

1. The sandstone specimens showed obvious deterioration under the effect of chemical solutions. During the corrosion, the stress-strain curves of the specimens gradually moved downward and to the right as the corrosion duration increased. The

brittleness of the specimens gradually declined, and their plasticity significantly increased as the specimens transitioned from brittle to ductile states.

2. Chemical damage deteriorated the specimens' microstructures. Deterioration gradually increased as the chemical damage duration increased. The accumulated corrosion damage deteriorated the physical mechanical properties to various extents. Deterioration damage to the mechanical properties differed in different chemical solutions; the damage degree deterioration of the internal friction angle was the least and that of K_{Ic} was the greatest.
3. There were consistent relations among the degrees of damage to mechanical and physical properties and the ion concentrations dissolved in the various chemical solutions. The greater the ion concentration in a chemical solution, the greater the deterioration of the physical and mechanical characteristics of the specimens.
4. The damage variable was defined to quantitatively analyze the degree of damage to the sandstone based on the change in its porosity. The relations among K_{Ic} , uniaxial compressive strength, tensile strength, and the damage variable were negative exponential functions, whereas the relations among the cohesiveness, internal friction angle, P-wave velocity, and the damage variable were negative linear functions.

Acknowledgements

The authors gratefully acknowledge the support of the National Natural Science Foundation of China (Nos. 11302167, 11572244, and 51478272), the joint funds of the National Natural Science Foundation and Guangdong Province of China (U1301241), the International Cooperation and Exchange of the National Natural Science Foundation of China (51520105012), and the Collaborative Innovation Research Centre for Environment-Friendly Materials and Structures in Civil Engineering, Southeast University, the Science and Technology Foundation for the Basic Research Plan of Shenzhen City (JCYJ20160422095146121).

Publisher's Note Springer Nature remains neutral with regard to jurisdictional claims in published maps and institutional affiliations.

REFERENCES

- Ayatollahi, M. R., & Aliha, M. R. M. (2007). Fracture toughness study for a brittle rock subjected to mixed mode I/II loading. *International Journal of Rock Mechanics and Mining Sciences*, *44*, 617–624.
- Brown, H. J., & Reddish, D. J. (1997). Experimental relations between rock fracture toughness and density. *International Journal of Rock Mechanics and Mining Science*, *34*(1), 153–155.
- Chen, Y., Cao, P., & Chen, R. (2010). Effect of water–rock interaction on the morphology of a rock surface. *International Journal of Rock Mechanics and Mining Sciences*, *47*, 816–822.
- Chen, M., Jin, Y., & Yuan, C. Y. (2001). Study on the experimental for fracture toughness under confining pressure. *Mechanics and Engineering*, *23*(4), 32–35.
- Chen, M., & Zhang, G. Q. (2004). Laboratory measurement and interpretation of the fracture toughness of formation rocks at great depth. *Journal of Petroleum Science and Engineering*, *41*, 221–231.
- Ciccotti, M., Gonzato, G., & Mulargia, F. (2000). The double torsion loading configuration for fracture propagation: An improved methodology for the load-relaxation at constant displacement. *International Journal of Rock Mechanics and Mining Sciences*, *37*(7), 1103–1113.
- Cui, Z. D., Liu, D. A., An, G. M., et al. (2010). A comparison of two ISRM suggested chevron notched specimens for testing mode-I rock fracture toughness. *International Journal of Rock Mechanics and Mining Sciences*, *47*, 871–876.
- Deng, H. F., Zhu, M., Li, J. L., Wang, Y., Luo, Q., & Yuan, X. F. (2012). Study of mode-I fracture toughness and its correlation with strength parameters of sandstone. *Chinese Journal of Rock and Soil Mechanics*, *33*(12), 3585–3591.
- Erarslan, N., & Williams, D. J. (2012). The damage mechanism of rock fatigue and its relationship to the fracture toughness of rocks. *International Journal of Rock Mechanics and Mining Sciences*, *56*, 15–26.
- Feng, X. T., Chen, S. L., & Li, S. J. (2001). Effects of water chemistry on micro cracking and compressive strength of granite. *International Journal of Rock Mechanics and Mining Sciences*, *38*(4), 557–568.
- Feng, X. T., Ding, W. X., & Zhang, D. X. (2008). Multi-crack interaction in limestone subject to stress and flow of chemical solutions. *International Journal of Rock Mechanics and Mining Science*, *46*(1), 159–171.
- Han, T. L., Shi, J. P., Chen, Y. S., & Cao, X. S. (2018). Quantifying microstructural damage of sandstone after hydrochemical corrosion. *International Journal of Geomechanics*, *18*(10), 04018121.
- Han, T. L., Shi, J. P., Chen, Y. S., et al. (2015). Salt solution attack induced mechanical property degradation and quantitative analysis method for evolution of meso-structure damages of mortar. *Chinese Journal of Materials Research*, *29*(12), 921–930.

- Heggeheim, T., Madland, M. V., Risnes, R., et al. (2005). A chemical induced enhanced weakening of chalk by seawater. *Journal of Petroleum Science and Engineering*, 46(3), 171–184.
- Li, N., Zhu, Y. M., Bo, S., & Gunter, S. (2003). A chemical damage model of sandstone in acid solution. *International Journal of Rock Mechanics and Mining Sciences*, 40(2), 243–249.
- Nara, Y., Morimoto, K., Hiroyoshi, N., et al. (2012). Influence of relative humidity on fracture toughness of rock: Implications for subcritical crack growth. *International Journal of Solids and Structures*, 49, 2471–2481.
- Négrel, P., Millot, R., Roy, S., et al. (2010). Lead isotopes in groundwater as an indicator of water-rock interaction (Masheshwaram catchment, Andhra Pradesh, India). *Chemical Geology*, 274(3–4), 136–148.
- Reinhardt, H. W., & Mielich, O. (2014). Fracture toughness of alkali-sensitive rocks in alkaline solution. *International Journal of Rock Mechanics and Mining Sciences*, 70, 552–558.
- Saadaoui, M., Reynaud, P., & Fantozzi, G. (2000). Slow crack growth study of plaster using the double torsion method. *Ceramics International*, 26(4), 435–439.
- The Professional Standard Compilation Group of People's Republic of China, DL/T5368. (2007). *Specifications for rock tests in water conservancy and hydroelectric engineering*. Beijing: China Water Power Press. (In Chinese).
- Vezzù, K., Bertuccio, A., & Lucien, F. P. (2008). Numerical modelling of uniaxial compressive failure of granite with and without saline porewater. *International Journal of Rock Mechanics and Mining Sciences*, 45(7), 1126–1142.
- Wang, Y. X., Cao, P., Chen, Y., Wan, L. H., Huang, Y. H., Zhao, Y. L., et al. (2011a). Test study on damage and fracture mechanical effects for swelling soft rock during water corrosion. *Journal of Central South University (Science and Technology)*, 42(6), 1685–1691.
- Wang, Q. Z., Feng, F., Ni, M., et al. (2011b). Measurement of mode I and mode II rock dynamic fracture toughness with cracked straight through flattened Brazilian disc impacted by split Hopkinson pressure bar. *Engineering Fracture Mechanics*, 78(12), 2455–2469.
- Wu, X. D. (2013). Experimental study on the time-dependent behaviour of Xiangjiaba sandstone. *Applied Mechanics and Materials*, 256–259, 174–178.
- Zhang, Z. X. (2002). An empirical relation between mode I fracture toughness and the tensile strength of rock. *International Journal of Rock Mechanics and Mining Sciences*, 39(3), 401–406.
- Zhang, S., & Wang, Q. Z. (2009). Determination of rock fracture toughness by split test using five types of disc specimens. *Rock and Soil Mechanics*, 30(1), 12–18. (In Chinese).
- Zhang, F. C., Wang, X. C., Lu, J., et al. (1981). *Fracture mechanics* (pp. 49–56). Beijing: China Architecture and Building Press.
- Zhang, S., Wang, Q. Z., & Xie, H. P. (2008). Size effect of rock dynamic fracture toughness. *Explosion and Shock waves*, 28(6), 544–551.

(Received December 29, 2018, revised May 27, 2019, accepted May 29, 2019, Published online June 6, 2019)